SAE INTERNATIONAL

Analyzing In-cylinder Flow Evolution and Variations in a Spark-Ignition Direct-Injection Engine Using Phase-Invariant Proper Orthogonal Decomposition Technique

2014-01-1174

Published 04/01/2014

Hao Chen and Min Xu
Shanghai Jiao Tong Univ.

David L.S. Hung
Univ. of Michigan - SJTU Joint Institute

CITATION: Chen, H., Xu, M., and Hung, D., "Analyzing In-cylinder Flow Evolution and Variations in a Spark-Ignition Direct-Injection Engine Using Phase-Invariant Proper Orthogonal Decomposition Technique," SAE Technical Paper 2014-01-1174, 2014, doi:10.4271/2014-01-1174.

Abstract

The preparation of fuel-air mixture and its efficient, clean, and reliable combustion in spark-ignition direct-injection (SIDI) engines depend to a large extend on the complex in-cylinder air flow. It has been widely recognized that the ensemble-averaged flow field provides rather limited understanding of in-cylinder air motion due to the strong cycle-to-cycle variations. In this study, time-resolved particle image velocimetry (PIV) is utilized to measure the in-cylinder air motion in a motored single-cylinder optical engine. Then, the velocity fields from different phases (crank-angle positions during intake and compression strokes) of 200 engine cycles are analyzed using phase-invariant proper orthogonal decomposition (POD) technique. With the phase-invariant POD method, the velocity fields from different phases are decomposed into a single set of POD modes. In this manner, the POD modes can be used to represent any phase of the flow. In addition, the changes of the POD coefficients over different phases demonstrate how the flow evolves within engine cycles. Simultaneously, the coefficients from the 200 cycles for the same phase quantify the variation among different cycles. The first two phase-invariant POD modes extract the strong intake flow structures, and the third mode contains the flow structure during the compression stroke. Overall, the insight of in-cylinder flow evolution and its cycle-to-cycle variations can be further elucidated through the analysis of phase-invariant POD modes and their coefficients.

Introduction

To a large extent, the fuel-air mixing, flame kernel formation, and combustion process rely on the in-cylinder air motion in the spark-ignition direct-injection (SIDI) engines[1].Therefore, the in-cylinder air flow significantly influences the engine performance, fuel economy and harmful emission levels.

Hill et al[2] and Lee et al[3] investigated the effect of large scale in-cylinder air motions, such as tumble motion, on the combustion quality in spark-ignition (SI) engines. Tumble flow, which is defined as the coherent large scale flow structure rotating orthogonally to the engine cylinder axis, can be easily generated by the intake valves locating offset from axis of the engine cylinder[4, 5, 6, 7]. For several decades, SI engines usually introduce tumble vortex during the intake stoke, and then increase the turbulence intensity due to the breakdown of tumble structure at the end phase of compression stroke[8].

The enhanced turbulence intensity before ignition timing results in a more homogeneous fuel-air mixture and much faster flame speed. Rapid combustion reduces the available time for heating the end gas ahead of the spreading flame and lowers the knock tendency. Since engine knocking is a major factor that restricts the compression ratio of the SI engines, reducing knock tendency allows the compression ratio to increase, and therefore the thermal efficiency can be improved. In addition, the faster burning speed reduces the cycle-to-cycle variation[9], which allows the engine to operate at highly optimized cycles.

The large-scale flow motions (such as tumble) affect the fuel spray during intake stroke by carrying fuel droplets and vapor down to one side across the cylinder bottom and up to the other side repeatedly. In the meantime, the turbulence transports the in-cylinder charge at small scales, together with the large-scale motion, to make the mixture more homogeneous. Due to the insufficient space as the piston is moving upward at the late phase of compression stroke, the organized, large-scale motion breaks up into small-scale turbulence. In this way, the turbulence intensity is amplified.

However, as many researchers have pointed out, this in-cylinder flow process encounters large cycle-to-cycle variation[10, 11], and both the flow evolution and variations are not well understood[12, 13]. The proper orthogonal decomposition (POD), which has been utilized as a powerful analysis tool for engine cyclic variation research for over a decade [14, 15, 16, 17, 18], has the potential to fulfill this need. Generally, POD is performed on velocity fields achieved at the fixed crank-angle degree (CAD) from many engine cycles [19, 20]. POD extracts the organized flow coherent structures from the velocity fields of same CAD originated from different engine cycles. POD's kinetic energy-weighted feature allows the complex flow to be represented by a small number of POD modes, and the cyclic variation for that crank-angle position can be studied by analyzing the POD modes and their associated POD coefficients. As the elucidation and application of POD are confounding, our previous studies[21, 22] have offered a practical guide on performing POD on the engine flows, in which a compact MATLAB code has also been provided.

Fogleman et al [23] proposed the phase-invariant POD, in which the POD on velocity fields was performed within a time-varying domain, such as CADs intra cycles. In this manner, a set of POD modes representing any CAD of the flow could be obtained. However, their research was conducted in a cubic chamber with a square piston, but not in an actual engine configuration. Very recently, Liu et al [16] and Abraham et al [24] performed phase-invariant POD on both the experimental dataset (high-speed PIV) and simulation (large eddy simulation, LES) with the attempt to (1) investigate the flow evolution and variations; and (2) validate the cyclic varied LES flow fields by the cycle-to-cycle varying PIV data.

In this study, high-speed PIV is conducted in a single-cylinder SIDI optical engine. The velocity fields of 41 CADs during intake and compression strokes from 200 consecutive cycles are analyzed using the phase-invariant POD method. The physical meanings of the first three POD modes are interpreted. This objective of this study is to provide the insight into the flow evolution and variations during intake and compression strokes.

Experimental Apparatus & Setup

The SIDI single-cylinder optical engine employed in this study is depicted in Fig. 1. The engine was primarily composed of a prototype, double-overhead camshaft, four-valve, pent-roof cylinder head, and the AVL customized crank case. The optical access into the combustion chamber was obtained by three locations: (1) full-quartz liner, (2) two pent-roof windows exposing the engine head clearance volume, and (3) quartz piston with Bowditch[25] arrangement, combined with the mirror tilted at 45° to provide the view up through the piston window. The head arrangement of the single cylinder engine is depicted in Fig. 2. An eight-hole SIDI fuel injector and a spark plug were centrally installed in close proximity of each other. The engine had a stroke of 94.6 mm, a bore of 86 mm, and a compression ratio of 11:1. For the experiments in this study, an AVL AC dynamometer was used to motor the engine at 800 rpm. The AVL customized balance system was used to ensure the engine was running at the lowest possible vibration level.

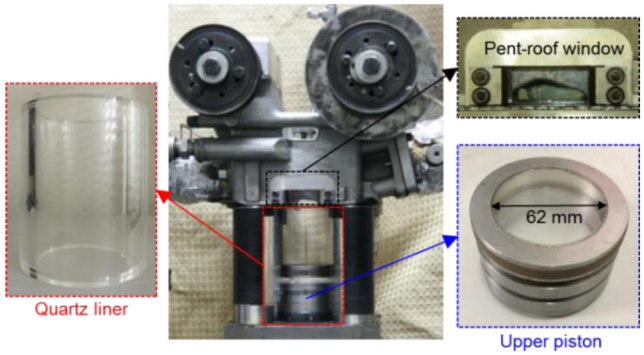

Figure 1. Optical engine

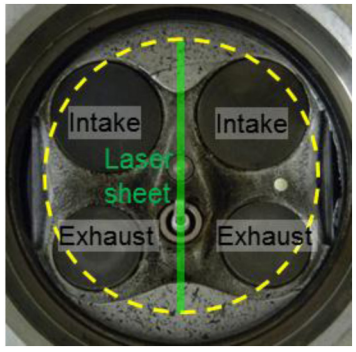

Figure 2. Bottom view of engine head (the dashed circle shows the optical view through quartz piston)

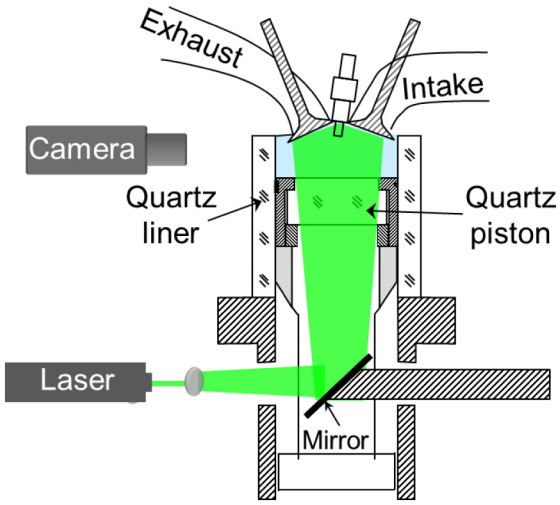

Figure 3. High-speed PIV experimental setup

Table 1 tabulates the engine parameters and the operating conditions. The electronic controlled throttle was used to adjust the intake air pressure. The engine intake air control system provided the intake air temperature of 25±1 °C. The AVL-577 Cooling Water and Lube Oil Supply Unit controlled the oil and coolant temperatures at 30 °C. The intake swirl level was regulated by adjusting the swirl valve mounted on one of the intake ports[9, 26]. In this test, the low swirl intake flow condition (swirl ratio = 0.55) was achieved by completely opening the swirl control valve.

Figure 3 depicts the experimental apparatus. Silicone oil droplets of about 1 μm diameter, generated by the TSI 6-jet atomizer, were introduced into the intake air as the PIV tracer. A Nd:YLF laser (527 nm wavelength, 24mJ/pulse @ 1000 Hz, 100 ns pulse width) was utilized to illuminate the tracers in the tumble plane, which bisected the combustion chamber and cut through the plane where the injector and spark plug were aligned. The laser sheet location is depicted in Figure 2. Mie-scattered images of tracer were recorded using a CMOS high speed camera (Vision Research, Phantom v7.3). The High-Speed Controller (HSC, LaVision) was employed to synchronize the image acquisition system with the engine signals. The recording rate was set at 1000 Hz, which corresponded to one velocity field for each 4.8 CAD at 800 rpm. For each cycle, spray images were recorded from −328.8° to −31.2° ATDCF (After TDC Firing). Velocity fields of 200 consecutive engine cycles were obtained.

The PIV data was processed using the commercial software LaVision DaVis 8.1. To obtain the best quality of the velocity fields, the following optimizations were made: First, the time delay between two PIV images was fixed throughout the cycle, and was optimized to realize the particle movement within ¼ of the final interrogation window[27, 28]. Second, the tracer density was adjusted to be 8~15 particles per interrogation window[27, 29]. Accordingly, Megerle et al. [29] reported about 2% precision for the PIV measurement. It is estimated that this level of PIV error would affect the POD energy spectrum by about 0.04% (which is the square of the precision of PIV measurements). Therefore, it has negligible effect on the low-order POD modes. Finally, the velocity fields were processed using the phase-invariant POD technique.

Table 1. Engine parameters

Parameter	Value
Displaced volume	549.51 cm^3
Stroke	94.6 mm
Bore	86 mm
Connecting Rod	160 mm
Compression ratio	11:1
Exhaust Valve Open (EVO)	131° ATDCF
Exhaust Valve Close (EVC)	372° ATDCF
Intake Valve Open (IVO)	-366° ATDCF
Intake Valve Close (IVC)	-114° ATDCF
Intake manifold absolute pressure	100 kPa
Intake air temperature	25 ± 1 ºC
Oil & Coolant temperature	30 ± 1 ºC
Intake swirl ratio	0.55

Proper Orthogonal Decomposition

Here, the POD procedure is briefly discussed. Detailed information and a compact POD code can be found in several previous papers by the authors[21, 22]. In this study, the mathematical procedure for phase-invariant POD is exactly the same as that in our previous phase-dependent POD. The only difference is that the input velocity fields here are the velocity fields from different CADs of 200 consecutive cycles, rather than those from the same CAD of different cycles for phase-dependent POD.

Conceptually, POD performs an optimal linear decomposition of a given set of velocity fields, $V^{(k)}$, k = 1,2, …, K, generates an orthonormal spatial basis functions (POD modes φ_m, m = 1,2, …, M) and associated coefficients $c_m^{(k)}$.

$$V^{(k)} = \sum_{m=1}^{M} c_m^{(k)} \varphi_m \tag{1}$$

where φ_m is the POD modes (coherent structures), with the number of modes, M, equals the input velocity fields number, K. Details of the MATLAB code described in previous paper [21] has been employed here. The code mathematically minimizes the following condition:

$$\sum_{k=1}^{K} \left\| V^{(k)} - \sum_{m=1}^{M'} c_m^{(k)} \varphi_m \right\|^2 \rightarrow \min \tag{2}$$

Equation (2) is realized by solving the eigenvalue problem of correlation matrix C ($C = \frac{1}{K} V V^T$).

$$C\beta_m = \lambda_m \beta_m \tag{3}$$

The eigenvectors (β_m, m = 1,2, …, M) are ranked with a decreasing order of corresponding eigenvalues (λ_m, m = 1,2 … M). This arrangement is meaningful so only the first several POD modes can capture the majority of the total kinetic energy. The basis functions are computed by projecting V on the eigenvector which are then normalized.

Finally, the coefficients of POD modes are computed by projecting the input velocity fields on basis functions. Since the POD modes are normalized, the coefficients $c_m^{(k)}$ contains the kinetic energy that the basis function, φ_m, contributes to the input velocity field, $V^{(k)}$. The kinetic energy captured by m^{th} mode from all K input velocity fields is:

$$KE_m = \frac{1}{2} \sum_{k=1}^{K} (c_m^{(k)})^2 \tag{4}$$

The energy fraction of the m^{th} mode is given by

$$ke_m = KE_m / \sum_{m=1}^{M} KE_m \tag{5}$$

It is worth mentioning that the summation of kinetic energy in all *M* POD modes (Equation 4) is equal to the summation of kinetic energy in all *K* input velocity fields [21, 22]. Performing POD on a set of synthetic velocity fields is very helpful to clarify the physical meaning of POD technique [22].

In this study, comparison of two velocity fields is often required. Since visual comparison of two flow pattern is subjective and highly qualitative, the relative index [17, 21, 22], R_p, which is computed by projecting one velocity field $V^{(1)}$ on another $V^{(2)}$ is employed to make quantitative comparison.

$$R_p = \left| \frac{(V^{(1)}, V^{(2)})}{\|V^{(1)}\| \|V^{(2)}\|} \right| \tag{6}$$

Because of the normalization step (the denominator in Eq. 6), R_p varies from zero to one. When R_p equals 1, it represents a condition in which two flow patterns are exactly the same. When R_p is equal to 0, the two patterns are completely different. Figure 4 illustrates how the relevance index works. $V^{(1)}$ and $V^{(2)}$ have different flow patterns, thus, the relevance index between them is only 0.2511. $V^{(3)}$ is obtained by multiplying every vector in $V^{(2)}$ by a factor of 1.5. Therefore, while $V^{(2)}$ and $V^{(3)}$ possess the exact same flow pattern, their energy contained is different. So the relevance index between $V^{(2)}$ and $V^{(3)}$ is 1. In summary, R_p offers a single value which objectively and quantitatively compares the similarity degree of two flow patterns without regard to the energy amount.

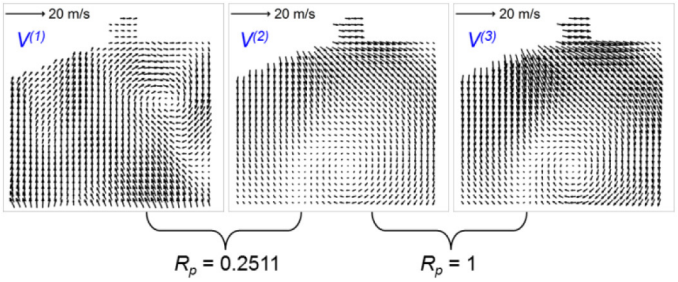

Figure 4. Relevance index between flow patterns

Results and Discussions

The main purpose of this study is to simultaneously investigate the flow evolution and variations during the intake and compression strokes in a quantitatively manner. To this end, this section is organized as follows. First, the flow evolution is described using the ensemble-averaged velocity fields. Then, the cyclic variation of flow is illustrated. Finally, the phase-invariant POD is conducted on the velocity fields of 41 CADs using 200 consecutive cycles to quantitatively analyze the flow evolution and cycle-to-cycle variations.

Ensemble-Averaged Velocity Fields Analysis

Figure 5 depicts the ensemble-averaged velocity fields at different CADs during the intake stroke. To display the flow structure clearly, the streamline is overlaid as shown in Figure 5. The air motion is measured at each velocity field per every 4.8 CAD. Only velocity fields at eight different CADs are shown in Figure 5. At −328.8° ATDCF, the intake air entered the cylinder through the intake valves with the maximum velocity of about 7m/s, and a vortex was formed below the intake valves.

As the intake valve opened, the velocity increased. Until −295.2°, the maximum velocity increased to about 27m/s. At −280.8°, after the intake valves had been fully open, the flow started to become weaker. In addition, the tumble vortex center formed at this CAD as highlighted by the dashed circle. From −280.8° to −252.0°, the tumble center moved to lower left, and the flow became weaker. After this CAD, the vortex center left the field of view, and the maximum velocity decreased to about 12m/s. Thetransition to the weaker flow can be attributed to the following reasons: (1) As the intake valves were fully open, the air could get through the valves by a larger area; (2) The flow interacted with the surfaces of the cylinder, piston, etc. Also, the flow structures interacted with each other.

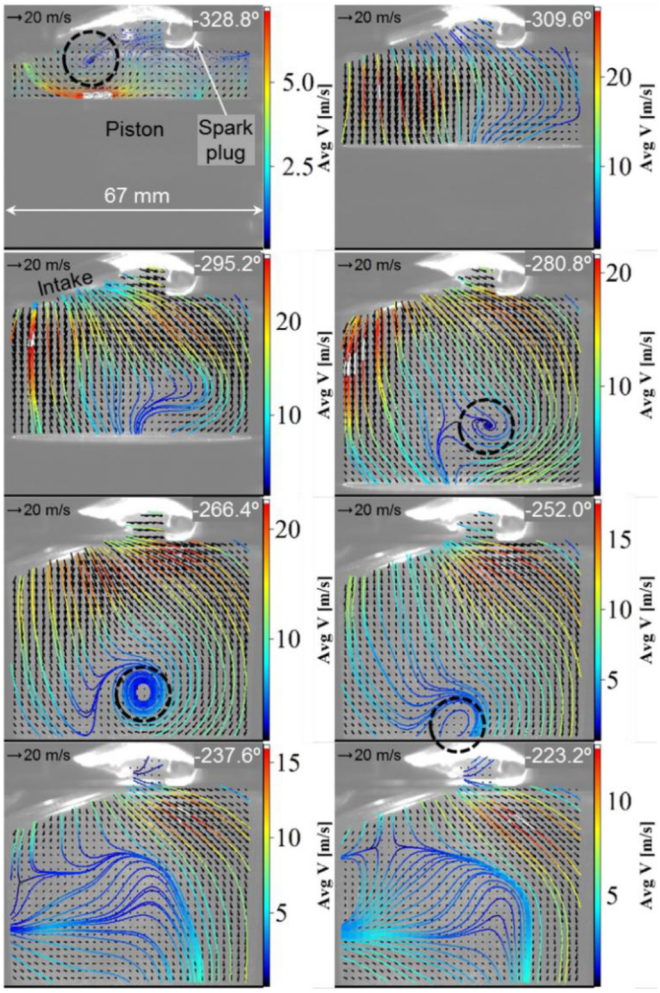

Figure 5. Ensemble-averaged (over 200 cycles) velocity fields during the intake stroke

Figure 6 depicts the ensemble-averaged velocity fields at eight different CADs during the compression stroke. Note that the velocity at compression was smaller than the velocity during intake stroke. To clearly show the vectors, the scale in Figure 6 was scaled up three times compared to the scale shown in Figure 5 for the same 20m/s. At early compression of −136.8°, the velocity magnitude was between 0 m/s to 3.5 m/s. As the piston moved upwards at −122.4°, the tumble vortex center

appeared in the right-lower corner, as highlighted by the dashed circle in Figure 6. From −108.0° to −64.8°, the tumble center moved to upper right location. Until about −50.4°, the center was out of view. Since the right side of field of view was only 12mm away from the cylinder wall, based on this moving speed, the tumble center would approach the cylinder wall and break down to small-scale motions after 5 to 8 CAD. Therefore, the tumble motion could not be found at the CAD of −31.2°. During the compression, the velocity magnitude was found to be between 0 m/s and 5 m/s.

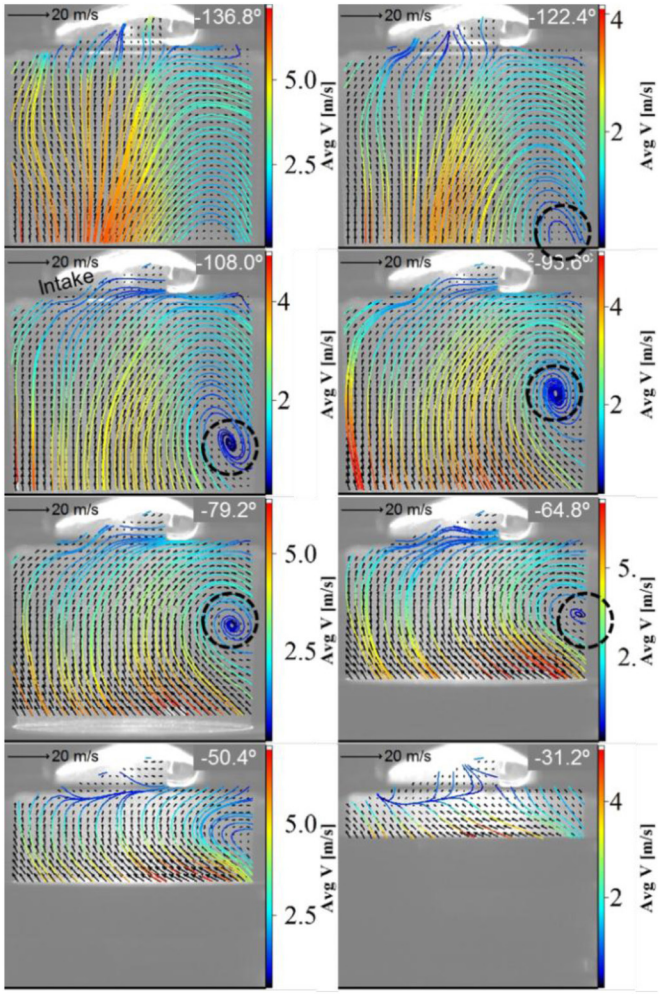

Figure 6. Ensemble-averaged (over 200 cycles) velocity fields during the compression stroke

Cycle-to-Cycle Variations

In the previous section, the flow evolution has been demonstrated using the ensemble-averaged flow fields. However, the ensemble-averaged flow is usually not qualified to fully represent the flow fields of any single cycle. Figure 7 shows the ensemble-averaged velocity field, and flow fields from three different cycles at −266.4° (during intake stroke). Clearly, the tumble center was different among different cycles, and it was clearly different than the ensemble-averaged flow, in which even two centers appeared in cycle #177. Since there was always a strong intake motion for all cycles, the variation during intake was expected to be smaller. The variation at compression stroke is anticipated to be larger, as shown in Figure 8. First, the flow patterns from different cycles were very different. Second, with the exception of a vortex center appearing at the similar location as that in the ensemble-averaged flow for cycle #13, cycle #1 did not show an identifiable vortex center, and cycle #45 had vortex center located at about 15mm far from the center in the ensemble-averaged flow.

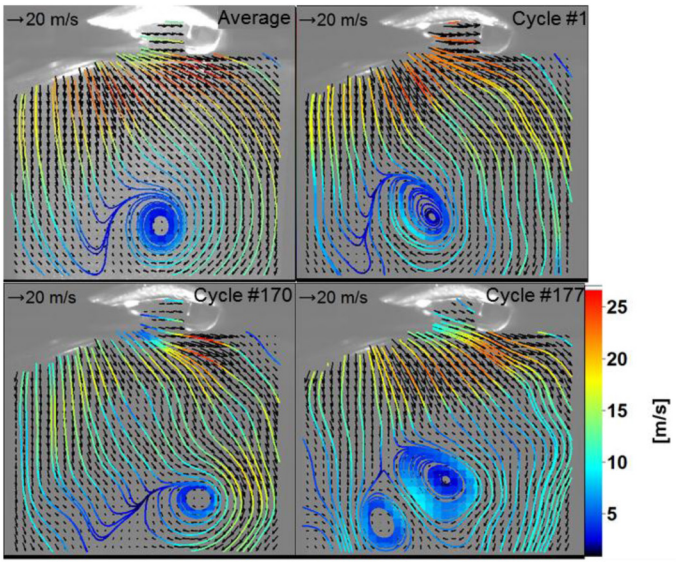

Figure 7. Ensemble-averaged flow (over 200 cycles), and velocity fields at −266.4° ATDCF from three different cycles

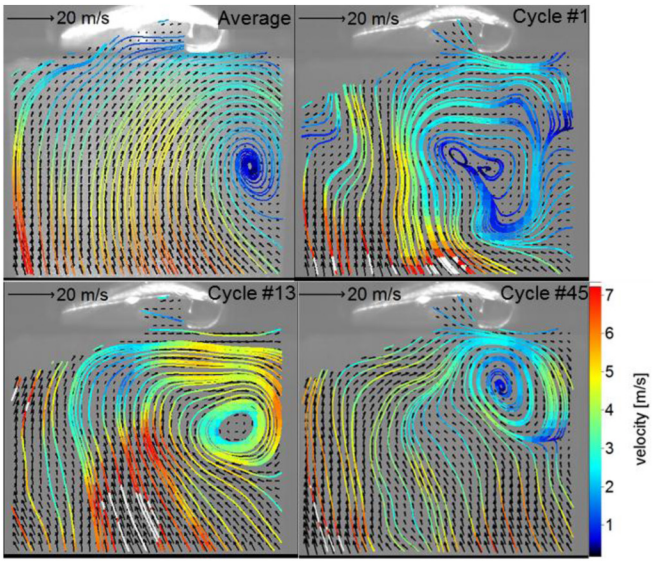

Figure 8. Ensemble-averaged flow (over 200 cycles), and velocity fields at −93.6° ATDCF from three different cycles

To further illustrate the variation in a quantitative manner, the relevance index is employed here. The velocity fields from 200 cycles are compared with their ensemble-averaged flow using relevance index between −266.4° and −93.6°, respectively. The results are depicted in Figure 9. As the R_p was about 0.9 with COV of 1.9% for −266.4°, it is clear that the flow varied much less during the intake stroke. This is because the dominated intake flow always appeared during intake stroke. In contrast, at −93.6° during the compression stroke, the R_p was found to vary between 0.60 and 0.95, demonstrating a larger variation during compression.

Overall, the air motion varies from one cycle to the next cycle, and novel means to evaluate the cycle-to-cycle variation other than ensemble average analysis is required.

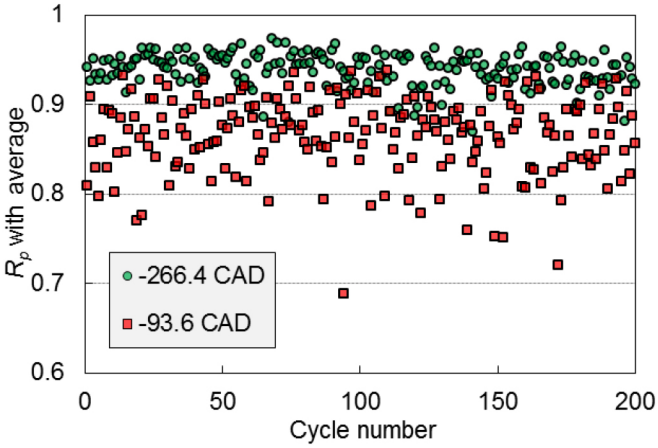

Figure 9. Relevance index between ensemble-averaged flow and velocity fields from 200 different cycles, for −266.4° and −93.6° respectively

Phase-Invariant POD Analysis

In this section, the phase-invariant POD is applied to the dataset of velocity fields (41 CADs × 200 cycles), in an attempt to quantitatively and simultaneously study the flow evolution and variations.

Figure 10 illustrates how the phase-invariant POD is performed in this study. The left side of the equation is the input snapshots, including the velocity fields from 41 different CADs (from intake to compression strokes, −276° to −84°ATDCF with an increment of 4.8°) of 200 cycles (overall 8200 velocity fields). The velocity fields of these CADs have equal number of vectors (grid points), and the piston was outside of the viewing area. Since the air density changes as a function of CADs, the mass-weighted coefficients should be multiplied to the velocity fields of different CADs. Figure 11 shows the mass-weighted coefficients computed using the ideal gas equation. After IVC, the air density increases as the piston moves upwards. The mass-weighted coefficients make sure that the velocity fields of different CADs represent the same amount of air mass. Phase-invariant POD creates modes (φ_1, φ_2, …) and coefficients as shown in the right side of Figure 10. In this manner, same mode (representing the organized flow structure) is achieved for the velocity fields at different CAD and different cycles. For the same mode, the coefficients comparison between different cycles at the same CAD demonstrated the cycle-to-cycle variation. Also, for the same mode, the coefficient comparisons between different CADs, illustrate the flow evolution. Moreover, only the first few modes would capture the energetic flow structures. Therefore, phase-invariant POD gives insight into the flow evolution and its variation simultaneously.

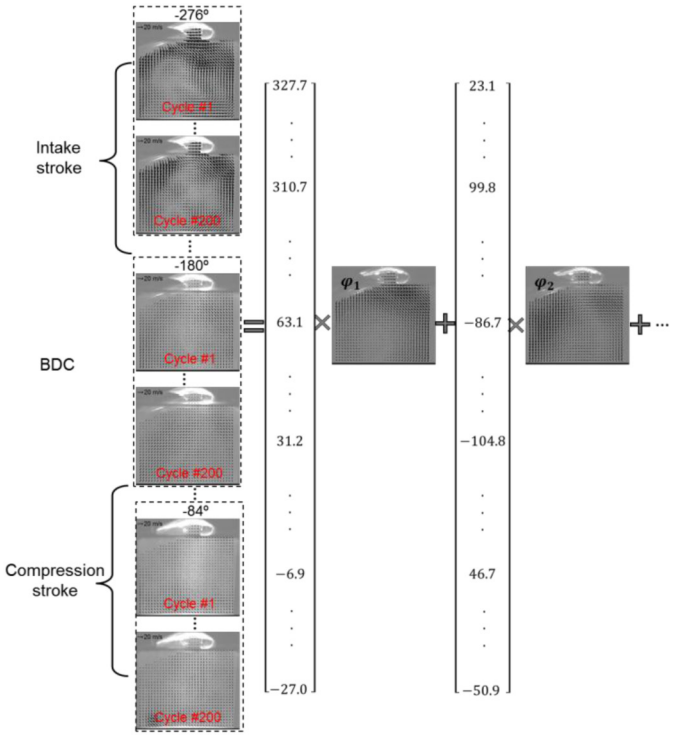

Figure 10. Illustration of phase-invariant POD

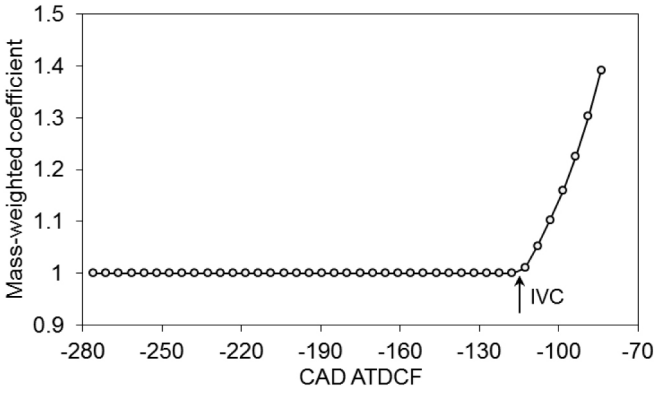

Figure 11. Mass-weighted coefficients for the velocity fields of different CADs

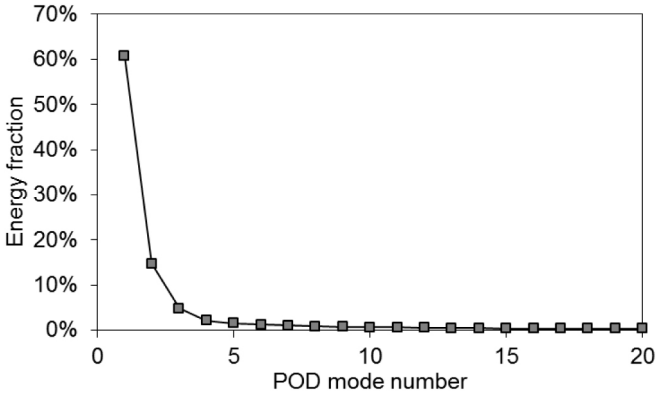

Figure 12. Kinetic energy fraction captured by the first 20 phase-invariant POD modes

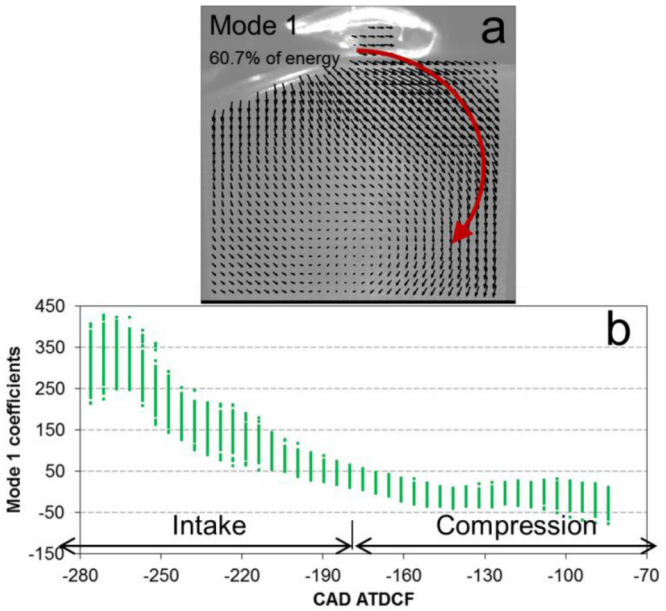

Figure 13. First POD mode and its coefficients evolution through intake and compression strokes. For each CAD, 200 coefficients illustrate the variation among 200 cycles

Figure 12 depicts the energy captured by the first 20 phase-invariant POD modes. The first three modes together captured more than 80% of the total energy (total kinetic energy from all 8200 input velocity fields). Therefore, only the physical meanings of the first three POD modes are investigated in this paper.

Figure 13 depicts the phase-invariant POD mode 1 and its coefficients of different CADs and different cycles. The first mode captures the intake flow which comes into the cylinder through the right side of the intake valve, as highlighted by the arrow in Figure 13. It is not surprising that this flow structure is the most energetic mode, since the intake air can enter the combustion cylinder without any obstacles at the right side the intake valves. In addition, as shown in Figs. 5 & 6, the intake flow is stronger than any other flow structures. Two observations can be made from the coefficients shown in Figure 13b. First, when comparing the coefficients at different CADs, it is clear that the coefficients decrease during the intake stroke. This is reasonable because the intake flow intensity decreases as shown in the previous section. The coefficients remain nearly zero during the compression stroke, suggesting that the compression stroke CADs do not possess this intake flow structure. Second, in comparison to the coefficients from different cycles at the same CAD, Figure 13b shows the cycle-to-cycle variations at different CADs. For instance, at −266.4°, the average coefficients and the COV of the 200 cycles are 339.2 and 10.8%, respectively. This provides quantitative information for the cyclic variation. Since the mode is normalized and only serves to show the flow pattern, the coefficients directly quantify the kinetic energy.

Figure 14 depicts the mode 2 and its coefficients. From Fig. 14a, it can be seen that mode 2 mainly captures the intake flow that enters the cylinder through the left side of the intake valve, as highlighted by the arrow in Fig. 14a. It can be computed from the coefficients that the kinetic energy contained in mode 2 is only about one quarter of that contained in mode 1, which quantitatively shows the intake flow intensity difference from the two directions. The intake flow from the left side of valve is weaker than of the right side. It is because the left side of the intake flow interacts with the left side of the cylinder wall, which is in close proximity to the intake valves. The decreasing values of mode 2 coefficients (Fig. 14b) also demonstrate that the intake flow is getting weaker during the intake stroke. In addition, the variation for this flow structure during intake is larger than that of first mode. For instance, at −266.4°, the average value and COV of the 200 coefficients are 66.4 and 39.0%, respectively. The COV is 4 times as large as that in the first mode, which has quantitatively demonstrated the variability.

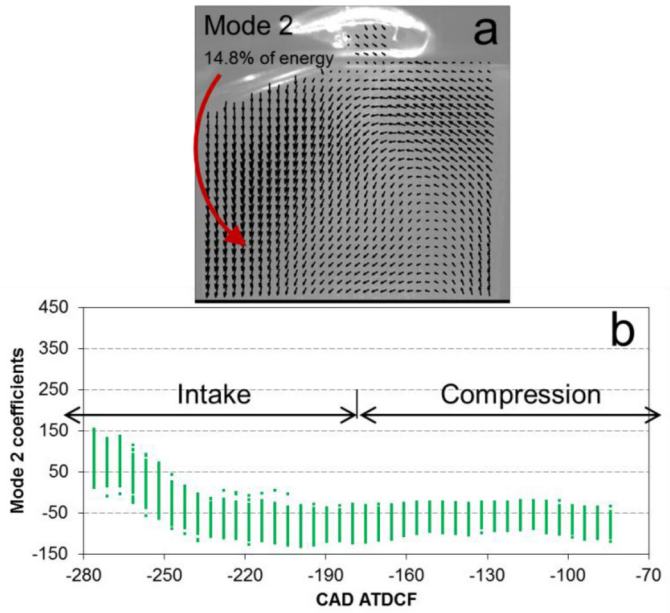

Figure 14. Second POD mode and its coefficients evolution through intake and compression strokes. For each CAD, 200 coefficients illustrate the variation among 200 cycles

Figure 15 shows the mode 3 and its coefficients. It can be seen that mode 3 mainly captures the flow due to the piston upward motion during compression stroke, which is highlighted in dashed circle in Figure 15a. In addition, the coefficients are negative during intake and they become positive during the compression stroke. It is because the flow during intake has opposite direction with the flow structure in mode 3, and flow direction is reversed due to upward motion of the piston at compression stroke. Overall, these results demonstrate that the phase-invariant POD method is a effective tool to analyze the flow evolution and variations at the same time.

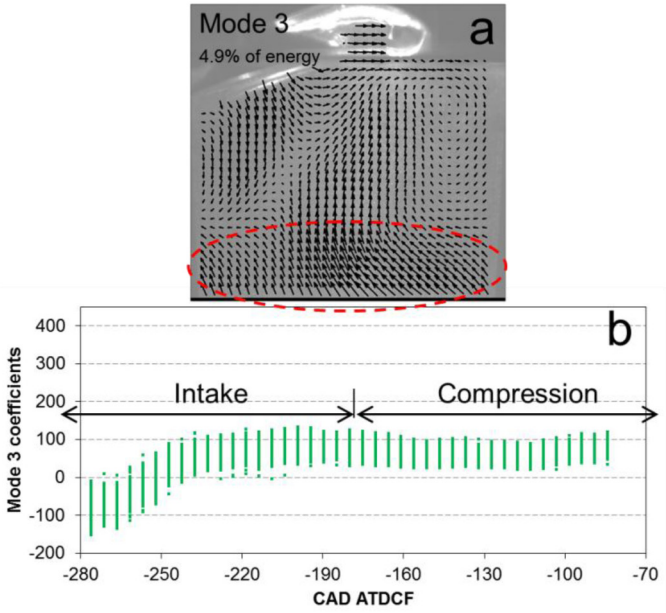

Figure 15. Third POD mode and its coefficients evolution through intake and compression strokes. For each CAD, 200 coefficients illustrate the variation among 200 cycles

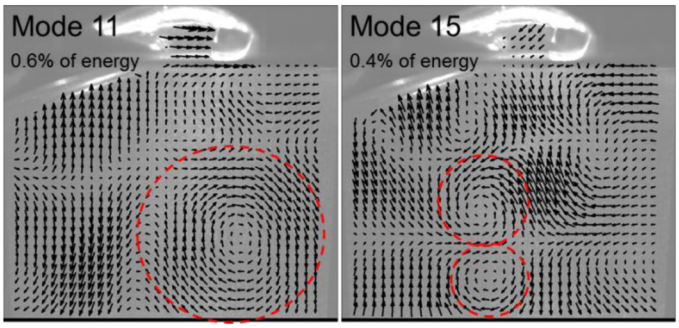

Figure 16. Phase-invariant POD of 11th & 15th modes

One may notice that the first three modes do not extract any vortical structures, which frequently appears within the flow fields (Figs. 5, 6, 7, 8). Due to the temporally and spatially intermittent nature of the vortical structure as well as their low energy, these eddies can only be seen (extracted) at the higher modes. Figure 16 shows the POD of 11th & 15th modes. The vortex patterns can be identified clearly in these modes, and their energy fraction is below 1% for both structures. Comparing the vortices in these two modes (highlighted with dashed circles), the large-scale eddy has more energy, and thus it usually appears in lower mode.

Summary and Conclusions

This paper provides an approach to simultaneously and quantitatively investigate the air flow evolution and cycle-to-cycle variations during the intake and compression strokes by means of phase-invariant POD technique. The high-speed PIV measurement was conducted in a single-cylinder optical SIDI engine. The PIV data provided the velocity fields from different CADs of 200 consecutive cycles. The PIV parameters were optimized to ensure a good quality of the velocity field data. At first, the flow evolution was analyzed using the conventional ensemble-averaged method. However, due to the high cycle-to-cycle variation, not much information could be drawn from the ensemble average analysis.

The velocity fields from 41 CADs (from the intake to the compression strokes) of 200 cycles were analyzed using the phase-invariant POD. Mass-weighted coefficients were multiplied to the velocity fields of different CADs prior to the phase-invariant POD analysis. In this way, the velocity fields of different CADs represent the same amount of air mass.

The first three modes captured more than 80% of the total kinetic energy contained in the overall 8200 velocity fields. Insightful information on the flow evolution and variation can be obtained from this method:

- Phase invariant POD decomposes the flow into several main flow structures, and their coefficients can be used to quantify the flow evolution and cycle-to-cycle variations.
- The first phase-invariant POD mode extracts the characteristics of the intake flow which is through the right side of the intake valve. The second mode captures the intake flow through the left side of the intake valve. The intake flow from right side is about 4.2 times stronger than that from the left side. This is caused by intake flow on the left side interacting with the left cylinder wall, which is very close to the intake valve. Thus, the flow from the left side is found to be much weaker.
- For the first two modes, the coefficients for the same CAD but different cycles can be used to quantify the cycle to cycle variation. For instance, at −266.4°, the COV of the 200 mode 1 coefficients is 10.8%. The COV is 39.0% for that of mode 2. It demonstrates in a quantitative manner that the intake flow on the left side (mode 2) interacts with cylinder wall, resulting in larger cyclic variation than the intake flow on the right side (mode 1) by a factor of about four.
- The third mode extracts the flow induced by the piston upward movement during the compression stroke. The mode coefficients continue to increase during compression stroke, illustrating that this flow structure is enhanced.
- Owing to the low energy of the smaller vortical structures, they can only be extracted in the higher modes. In general, large-scale eddies possess more energy, and so they appear in lower POD modes more clearly than the small-scale eddies.

Overall, the phase-invariant POD provides an effective way to simultaneously illustrate the flow evolution and quantify the cycle-to-cycle variations of the in-cylinder engine flow characteristics.

References

1. Zhao, F., Lai M.-C., and Harrington D.L., Automotive Spark-Ignited Direct-Injection Gasoline Engines. Progress in Energy and Combustion Science, 25(5): 437-562, 1999 doi:10.1016/S0360-1285(99)00004-0.

2. Hill, P.G. and Zhang D., The effects of swirl and tumble on combustion in spark-ignition engines. Progress in Energy and Combustion Science, 20(5): 373-429, 1994 doi:http://dx.doi.org/10.1016/0360-1285(94)90010-8.
3. Lee, K., Bae C., and Kang K., The effects of tumble and swirl flows on flame propagation in a four-valve S.I. engine. Applied Thermal Engineering, 27(11-12): 2122-2130, 2007 doi:http://dx.doi.org/10.1016/j.applthermaleng.2006.11.011.
4. Mittal, M., Hung, D., Zhu, G., and Schock, H., "High-Speed Flow and Combustion Visualization to Study the Effects of Charge Motion Control on Fuel Spray Development and Combustion Inside a Direct-Injection Spark-Ignition Engine," *SAE Int. J. Engines* 4(1):1469-1480, 2011, doi:10.4271/2011-01-1213.
5. Li, Y., Zhao H., Leach B., Ma T., and Ladommatos N., Characterization of an in-cylinder flow structure in a high-tumble spark ignition engine. International Journal of Engine Research, 5(5): 375-400, 2004 doi:10.1243/1468087042320924.
6. Li, Y., Zhao, H., Peng, Z., and Ladommatos, N., "Analysis of Tumble and Swirl Motions in a Four-Valve SI Engine," SAE Technical Paper 2001-01-3555, 2001, doi:10.4271/2001-01-3555.
7. Frieden, D. and Sick, V., "Investigation of the Fuel Injection, Mixing and Combustion Processes in an SIDI Engine using Quasi-3D LIF Imaging," SAE Technical Paper 2003-01-0068, 2003, doi:10.4271/2003-01-0068.
8. Lumley, J.L., *Engines, An Introduction*. 1999: Cambridge University Press.
9. Hung, D.L.S., Chen H., Xu M., Yang J., and Zhuang H.. *Experimental Investigation of the Variations of Early Flame Development in a Spark-Ignition Direct-Injection Optical Engine.Proceedings of the ASME 2013 Internal Combustion Engine Division Fall Technical Conference*, 2013.
10. Frieden, D. and Sick, V., "Investigation of the Fuel Injection, Mixing and Combustion Processes in an SIDI Engine using Quasi-3D LIF Imaging," SAE Technical Paper 2003-01-0068, 2003, doi:10.4271/2003-01-0068.
11. Funk, C., Sick, V., Reuss, D., and Dahm, W., "Turbulence Properties of High and Low Swirl In-Cylinder Flows," SAE Technical Paper 2002-01-2841, 2002, doi:10.4271/2002-01-2841.
12. Voisine, M., Thomas L., Borée J., and Rey P., Spatio-temporal structure and cycle to cycle variations of an in-cylinder tumbling flow. Experiments in Fluids, 50(5): 1393-1407, 2011 doi:10.1007/s00348-010-0997-7.
13. Liu, D., Wang T., Jia M., and Wang G., Cycle-to-cycle variation analysis of in-cylinder flow in a gasoline engine with variable valve lift. Experiments in Fluids, 53(3): 585-602, 2012 doi:10.1007/s00348-012-1314-4.
14. Druault, P., Guibert P., and Alizon F., Use of proper orthogonal decomposition for time interpolation from PIV data. Application to the cycle-to-cycle variation analysis of in-cylinder engine flows. Experiments in Fluids, 39(6): 1009-1023, 2005 doi:10.1007/s00348-005-0035-3.
15. Roudnitzky, S., Druault P., and Guibert P., Proper orthogonal decomposition of in-cylinder engine flow into mean component, coherent structures and random Gaussian fluctuations. Journal of Turbulence, 7(0): 1-19, 2006 doi:10.1080/14685240600806264.
16. Liu, K., Haworth D., Yang X., and Gopalakrishnan V., Large-eddy Simulation of Motored Flow in a Two-valve Piston Engine: POD Analysis and Cycle-to-cycle Variations. Flow, Turbulence and Combustion, 91(2): 373-403, 2013 doi:10.1007/s10494-013-9475-7.
17. Chen, H., Reuss D., and Sick V., Analysis of misfires in a direct injection engine using proper orthogonal decomposition. Experiments in Fluids, 51(4): 1139-1151, 2011 doi:10.1007/s00348-011-1133-z.
18. Chen, H., Hung D.L.S., Xu M., and Zhong J., Analyzing the Cycle-to-Cycle Variations of Pulsing Spray Characteristics by Means of the Proper Orthogonal Decomposition. Atomization and Sprays, 23(7): 623-641, 2013 doi:10.1615/AtomizSpr.2013007851.
19. Vu, T.-T. and Guibert P., Proper orthogonal decomposition analysis for cycle-to-cycle variations of engine flow. Effect of a control device in an inlet pipe. Experiments in Fluids, 52(6): 1519-1532, 2012 doi:10.1007/s00348-012-1268-6.
20. Kapitza, L., Imberdis O., Bensler H.P., Willand J., and Thevenin D., An experimental analysis of the turbulent structures generated by the intake port of a DISI-engine. Experiments in Fluids, 48(2): 265-280, 2010 doi:10.1007/s00348-009-0736-0.
21. Chen, H., Reuss D.L., Hung D.L., and Sick V., A practical guide for using proper orthogonal decomposition in engine research. International Journal of Engine Research, 14(4): 307-319, 2013 doi:10.1177/1468087412455748.
22. Chen, H., Reuss D.L., and Sick V., On the use and interpretation of proper orthogonal decomposition of in-cylinder engine flows. Measurement Science and Technology, 23(8): 085302, 2012 doi:10.1088/0957-0233/23/8/085302.
23. Fogleman, M., Lumley J., Rempfer D., and Haworth D., Application of the Proper Orthogonal Decomposition to Datasets of Internal Combustion Engine Flows. Journal of Turbulence, 5, 2004 doi:10.1088/1468-5248/5/1/023.
24. Abraham, P., Liu K., Haworth D., Reuss D., and Sick V., Evaluating Large-Eddy Simulation (LES) and High-Speed Particle Image Velocimetry (PIV) with Phase-Invariant Proper Orthogonal Decomposition (POD) Oil & Gas Science and Technology, 0(0): 1-19, 2013 doi:10.2516/ogst/2013126.
25. Bowditch, F., "A New Tool for Combustion Research A Quartz Piston Engine," SAE Technical Paper 610002, 1961, doi:10.4271/610002.
26. Chen, H., Xu, M., Hung, D., Yang, J. et al., "Development of a POD-Based Analysis Approach for Quantitative Comparison of Spray Structure Variations in a Spark-Ignition Direct-Injection Engine," SAE Technical Paper 2013-01-2545, 2013, doi:10.4271/2013-01-2545.

27. Keane, R.D. and Adrian R.J., Optimization of particle image velocimeters. Part I: Double pulsed systems. Measurement Science and Technology, 1(11): 1202-1215, 1990 doi:10.1088/0957-0233/1/11/013.

28. Keane, R.D. and Adrian R.J., Optimization of particle image velocimeters: II. Multiple pulsed systems. Measurement Science and Technology, 2(10): 963-974, 1991 doi:10.1088/0957-0233/2/10/013.

29. Megerle, M., Sick V., and Reuss D.L., Measurement of digital particle image velocimetry precision using electro-optically created particle-image displacements. Measurement Science and Technology, 13(7): 997-1005, 2002 doi:10.1088/0957-0233/13/7/305.

Contact Information

Hao Chen
chenhow2008@gmail.com

Min Xu
mxu@sjtu.edu.cn

David L.S. Hung
dhung@sjtu.edu.cn

Acknowledgments

This research is sponsored by General Motors R&D Corporation (USA) and National Natural Science Foundation of China (NSFC) under grants No. 51076093/E060702 and 51176115/E060404, and carried out at the National Engineering Laboratory for Automotive Electronic Control Technology of the Shanghai Jiao Tong University. Additional funding support on this research to D.L.S. Hung has also been provided by Shanghai Jiao Tong University Engineering-Science Interdisciplinary Research Fund and the 2009 Program for New Century Excellent Talents in University by the Ministry of Education (MOE), China.

ISSN 0148-7191

http://papers.sae.org/2014-01-1174